Environmental Science and Pollution Research (2023) 30:118693–118705
https://doi.org/10.1007/s11356-023-30628-z

RESEARCH ARTICLE

Investigating the transport and colloidal behavior of Fe_3O_4 nanoparticles in aqueous and porous media under varying solution chemistry parameters

Reetha Thomas[1] · Debayan Ghosh[1] · Mrudula Pulimi[1] · Joyce Nirmala[2] · Shalini Anand[3] · Pramod Kumar Rai[3] · Amitava Mukherjee[1]

Received: 21 July 2023 / Accepted: 19 October 2023 / Published online: 2 November 2023

Abstract

The possible adverse effects of engineered iron oxide nanoparticles, especially magnetite (Fe_3O_4 NP), on human health and the environment, have raised concerns about their transport and behavior in soil and water systems. Accumulating these NPs in the environment can substantially affect soil and water quality and the well-being of aquatic and terrestrial organisms. Therefore, it is essential to examine the factors that affect Fe_3O_4 NP transportation and behavior in soil and water systems to determine their possible environmental fate. In this work, experiments were conducted in aqueous and porous media using an environmentally relevant range of pH (5, 7, 9), ionic strength (IS) (10, 50, 100 mM), and humic acid (HA) (0.1, 1, 10 mg L^{-1}) concentrations. Fe_3O_4 NPs exhibited severe colloidal instability at pH 7 ($\sim = pH_{PZC}$) and showed an improvement in apparent colloidal stability at pH 5 and 9 in aquatic and terrestrial environments. HA in the background solutions promoted the overall transport of Fe_3O_4 NPs by enhancing the colloidal stability. The increased ionic strength in aqueous media hindered the transport by electron double-layer compression and electrostatic repulsion; however, in porous media, the transport was hindered by ionic compression. Furthermore, the transport behavior of Fe_3O_4 NPs was investigated in different natural waters such as rivers, lakes, taps, and groundwater. The interaction energy pattern in aquatic systems was estimated using the Derjaguin-Landau-Verwey-Overbeek (DLVO) theory. This study showed the effects of various physical–chemical conditions on Fe_3O_4 NP transport in aqueous and porous (sand) media.

Keywords Fe_3O_4 · DLVO theory · Aqueous environment · Porous media · Transport

Introduction

Iron oxide nanoparticles (Fe_3O_4 NPs) have remarkable characteristics such as superparamagnetic capabilities, large surface-to-volume ratio, and biocompatibility; thus, it is the choice of interest for many applications (Ali et al. 2016). Magnetite (Fe_3O_4) is one of the most prevalent forms of iron oxide occurring in nature (Elias and Alderton 2020). The engineered Fe_3O_4 NPs are generally acceptable for many applications such as sensor development, pigment production, biomedical imaging, ferrofluid technology, and environmental remediation (Imran et al. 2021; Kumar et al. 2021). Nevertheless, the extensive use of Fe_3O_4 NPs is potentially detrimental to aquatic biota and human life. Fe_3O_4 NPs are released into the aquatic and terrestrial environments through various anthropogenic processes. The fate of Fe_3O_4 NPs in the environment is influenced by their physical and chemical properties, such as size, shape, and crystal structure. For instance, the smaller magnetite particles can be transported further in the environment and are more mobile, but larger particles may settle more rapidly and accumulate in certain regions (Popescu et al. 2019; Vindedahl et al. 2016). The surface properties may also influence

Responsible Editor: Thomas D. Bucheli

Reetha Thomas and Debayan Ghosh have equal contributions.

✉ Amitava Mukherjee
amitav@vit.ac.in

[1] Centre for Nanobiotechnology, Vellore Institute of Technology, Vellore, Tamil Nadu 632014, India

[2] Department of Chemical Engineering, Indian Institute of Technology Madras, Chennai, India

[3] Centre for Fire, Explosive and Environment Safety, Timarpur, Delhi, India

their fate in the environment. For instance, natural organic matter (NOM) may be coated on the surface of Fe_3O_4 NPs, which may impact their ability to interact with other elements of the environment (Daoush 2017). After being released into the environment, Fe_3O_4 NPs are exposed to multiple environmental conditions of the aquatic and terrestrial systems, such as pH, ionic strength, flow velocity, pore size, and concentration of natural organic matter (NOM) (Goswami et al. 2017; Lei et al. 2018). These NPs may be deposited in porous media or transported via aqueous media once in the environment, potentially toxic to terrestrial and aquatic organisms (Naz et al. 2022; Ouyang et al. 2022; Yu et al. 2014). Different environmental factors, however, may impact the fate and toxicity of Fe_3O_4 NPs (Galloway et al. 2017; Kahlon et al. 2018).

The transport of NPs in aqueous and porous media significantly affects how they will behave in the environment and how they may affect the environment and human health. Several components, including IS and NOM, govern the transport in aqueous media. In contrast, transport in porous media is primarily determined by physical processes such as advection, diffusion, and retention in the pore spaces (Dibyanshu et al. 2022, Ling et al. 2021, Meng and Yang 2019). Multiple research groups have previously explored the effect of several environmentally significant physicochemical factors on the transport and behavior of Fe_3O_4 NPs (Chen et al. 2019; Fazeli Sangani et al. 2019; Wang et al. 2022). Surface charge and pH levels substantially impact NPs' behavior in the aqueous environment. The NPs' high surface charges at both high and low pH levels cause stronger electrostatic repulsion between them, which prevents them from aggregating. However, as the pH gets closer to the point of zero charge (PZC) for the particles, the surface charge of the particle gets shielded by the water ions, which diminishes electrostatic repulsion and ultimately raises the probability of aggregation (Chekli et al. 2013). Adding NOM enhanced the stability of iron oxide NPs in the aqueous environment. The higher environmental concentration of NOM triggered NP disaggregation due to the enhanced steric repulsion induced by the sorption of negatively charged NOM molecules (Baalousha 2009). The transport of Fe_3O_4 NPs in porous media presents distinctive hurdles owing to various factors, including their dimensions, surface properties, interactions with the solid matrix, and the coexistence of additional substances. These factors intricately affect the stability, aggregation, and deposition of the NPs, consequently shaping their fate and spatial distribution within the media. Li et al. investigated iron oxide's co-transport and retention behavior and different-sized plastic particles in saturated sand media. Their findings suggest that the steric repulsion, variation of retention sites on sand particles, and the modification of Fe_3O_4 surface properties were the factors governing the transport mechanism (Li et al. 2019). Another study by Carstens and coworkers evaluated the effect of flow interruption on iron oxide of organic matter–coated goethite (OMCG) colloids in quartz sand media. The main reason for deposition during flow retardation was colloidal capture at sites with desirable DLVO/XDLVO interactions, which was encouraged by quick colloidal settling onto the solid matrix (Carstens et al. 2017). However, there is little knowledge about the fate and transport of Fe_3O_4 NPs in real-world environmental conditions. Therefore, for determining their potential adverse effects on the environment and establishing efficient mitigation approaches, a thorough understanding of the transport of nanoparticles in both porous and aqueous media is essential. As previously mentioned, the transport behavior of Fe_3O_4 NPs under aqueous and porous media with diverse chemical conditions has been studied. A Fe_3O_4 concentration of 50 mg L^{-1} was considered to evaluate maximum environmental impact and transport behavior. Various solution chemistry (including pH, IS, and NOM) crucial to NP suspensions' stability, aggregation, and deposition was considered.

This study is the first to investigate the transport profile of Fe_3O_4 NPs in the aqueous and porous media, considering various environmentally relevant solution chemistry factors. The aggregation, transport, and deposition characteristics of Fe_3O_4 NPs in these environments were critically analyzed. It was hypothesized that several physicochemical factors will considerably influence the sedimentation and deposition patterns of Fe_3O_4 NPs, hence influencing its transport in aqueous and terrestrial environments. The Fe_3O_4 NPs were characterized by FT-IR, XRD, TEM, and EDAX techniques. In addition, the observed transport profiles were mathematically validated using the DLVO interaction energy modeling. Overall, this work aims to elucidate the transport of Fe_3O_4 NPs in porous and aqueous media, which can provide valuable insights into the behavior of Fe_3O_4 NPs in these environments, aiding in the development of appropriate risk assessment and management strategies.

Materials and methods

Materials and sample preparation

Fe_3O_4 NPs that were used in various biotechnological fields (Shukla et al. 2010) were provided by CFEES-DRDO, Timarpur, Delhi, India. Humic acid standards (CAS Number 14808–60–7) as a representative of NOM and white quartz sand (particle size 50–70 mesh) (CAS Number 14808–60–7) used in the column transport experiment were obtained from Sigma-Aldrich. Analytical research (AR) grade NaCl supplied by SRL India Pvt. Ltd was used to prepare the background solution in the study. Glass chromatography columns 20 × 1.5 cm (Econo-Column, Catalog No. 7371522) were

purchased from Bio-Rad. All tests (except the transport studies in natural waters) were performed with ultrapure Milli-Q water (18.2 MΩ cm at 25 °C) (Pall Corporation, Ann Arbor, MI, USA).

A suspension of Fe_3O_4 NPs (50 mg L^{-1}) was prepared freshly, and the suspension was ultrasonically dispersed for 30 min at 40 kHz to form a homogenous suspension (Ding et al. 2019). In the Milli-Q water, humic acid (HA) stock solution (100 mg L^{-1}) was prepared and kept on a rotary shaker for about 24 h. Solids were separated from the solution using a 0.45-µm membrane filter. A TOC analyzer (TOC-L, Shimadzu) was used to determine the total organic carbon concentration of the processed stock solution. The concentration (100 mg L^{-1}) was unchanged after filtering.

Nanoparticle characterization

The surface functional groups of Fe_3O_4 NPs were identified by FT-IR (IR Affinity-1, Shimadzu, Japan). To verify the crystallinity and phases of the Fe_3O_4 NPs, XRD (Advanced D8, Bruker, Germany) was performed. Fe_3O_4 NP samples dried under vacuum conditions were observed through FE-SEM (Thermo Fisher FEI Quanta 250 FEG) to characterize their size and surface morphologies. The absorption spectra of background solutions under each test condition were recorded using a UV–VIS spectrophotometer (UV-2600, Shimadzu). A 90 Plus Particle Analyzer (Brookhaven Instruments Corporation, USA) was also used to determine the hydrodynamic diameter and surface charge (ζ potential) of Fe_3O_4 NPs in each experimental condition.

Measurement of pH_{PZC}

The point of zero charge (pH_{PZC}) was investigated using the pH titration method (Herrera-Barros et al. 2020). A 0.01 M NaCl solution was prepared, and its pH was set to a range of 2, 4, 6, 8, and 10 (initial pH) by using NaOH/ HNO_3. One hundred milliliters of an aqueous solution was added with 50 mg L^{-1} of Fe_3O_4 NPs (the resulting concentration is 0.216 mM), and the mixture was subsequently shaken in a rotary shaker for 48 h. The supernatant was decanted after 48 h, and again, the pH of the solution was measured and designated as the final pH. The final pH *versus* the initial pH was plotted, and these curves' points of convergence revealed pH_{PZC}.

Transport experiments

Transport behavior of Fe_3O_4 NPs in aqueous media

A wide range of environmental conditions, including pH (5, 7, 9), IS (10, 50, 100 mM), and HA (10, 50, 100 mg L^{-1}), were employed to simulate and investigate the interactions and effects of various physiochemical factors. The aqueous transport of Fe_3O_4 NPs was emphasized based on sedimentation (Ma et al. 2018; Mondal et al. 2021). After ultrasonication, the colloidal suspension was kept on a steady platform to mimic the static conditions for about 5400 s. The samples from the surface layer were taken at an interval of 300 s (Lv et al. 2016). The collected suspension was measured using a UV–VIS spectrophotometer at 370 nm (Chaki et al. 2015). The sedimentation curve was analyzed by calculating the absorbance ratio (A/A_0) as a function of time (A_0 = initial absorbance and A = absorbance of Fe_3O_4 at the end of the sedimentation study) (Zheng et al. 2019). Additionally, after each experiment, the aggregation rate was determined by monitoring the variation in size distribution, and the stability of Fe_3O_4 suspensions was determined in terms of hydrodynamic size and ζ potential. The employment of varied parameters in combination with a comparison of particle stability in static conditions can significantly improve the overall comprehension of the transport profile of Fe_3O_4 NPs in the aqueous environment.

Transport behavior of Fe_3O_4 NPs in porous media

Further, the quartz sand (mesh size: 50–70) was selected for the porous media transport because of its uniform pore distribution, chemical stability, high porosity, and surface area (Tong et al. 2020). Moreover, it provides a standardized and consistent platform for understanding the transport behavior in porous media. Table S4 represents the specifications of the porous media. The glass chromatography columns were employed with a fixed bed of 20 cm height and 1.5 cm inner diameter (Bio-Rad, Econo-Column, Catalog No. 7371522). Before establishing the column, the sand was thoroughly washed with 0.1 M HCl, rinsed with Milli-Q water, and dried. The column was packed with quartz sand, which was packed uniformly into a 5-cm-high bed with gentle taps to ensure fine packing and then saturated. A peristaltic pump (Miclins PP-30-EX) was employed throughout the study, with the flow rate set to 1 mL/min in a downward direction. Further, the sand column's tubing factor and pore volume (PV) were calculated. The NP suspensions were first homogenized by probe sonication, followed by repeated introduction to the column through a silicon tube to obtain 4 PVs of the suspension. Furthermore, a background solution with a volume equal to 5 PV was used to rinse the column. Ultrapure water was added to the column till the effluents were completely free of NPs. The pH (5, 7, and 9), IS (10, 50, and 100 mM), and HA (0.1, 1, and 10 mg L^{-1}) were considered as the variables in this transport experiment. UV–VIS spectrophotometer analyzed all the PVs for the Fe_3O_4 NPs collected from the column. The calibration curves quantifying Fe_3O_4 transport were plotted using different concentrations obtained from the absorbance. The breakthrough curves (BTCs) were analyzed by calculating the concentration

ratio (C/C_0) as a function of PV (represents the volume of the porous medium), in which C_0 and C are the concentrations of the nanoparticles in influent and effluent, respectively.

Transport behavior of Fe_3O_4 NPs in various natural water systems

To investigate the transport of NPs in natural water systems, four different types of water, such as lake, river, tap, and groundwater, were used to simulate actual environmental conditions. The detailed physicochemical characteristics of different environmental water samples are represented in Table S1. The Fe_3O_4 NPs were added to each environmental water sample, serving as background solutions (50 mg L^{-1}) for transport studies. The pH of the water samples remained unchanged, before adding the NPs. This was done to maintain the natural water conditions and avoid any potential pH variations that could introduce confounding factors. All the experiments were conducted in triplicate at a constant room temperature of 25 ± 1 °C, and the data are reported as mean ± standard deviation to demonstrate the repeatability of the transport results.

Theoretical consideration

DLVO interaction energy modeling

The classical DLVO theory was considered to establish the total interaction energy (V_{Total}) encountered by two particles approaching each other (Lu et al. 2016). It outlines the factors that affect the behavior and transport of NPs in the porous media. The stability and aggregation of the NPs are governed by the sum of two interactive forces, namely, the van der Waals force of attraction (V_{VDW}) and electrical double-layer repulsion (V_{EDL}). The following expressions are used to calculate the V_{VDW} and V_{EDL} (Ghosh et al. 2022).

$$V_{Total} = V_{VDW} + V_{EDL} \tag{1}$$

$$V_{VDW} = -\frac{Aa_1a_2}{6h(a_1+a_2)(1+\frac{14h}{\lambda})} \tag{2}$$

where A = Hamaker constant (3.3×10^{-20} J), h = distance between two NPs, a_1 = radius of NP 1, a_2 = radius of NP 2, and λ = characteristic wavelength associated with the interaction of NPs (100 nm).

$$V_{EDL} = 64\pi\varepsilon\varepsilon_0\frac{a_1a_2}{a_1+a_2}\zeta^2\exp(-\kappa h) \tag{3}$$

$$\kappa^2 = \frac{4\pi e^2\sum z_i^2 n_i}{\varepsilon\varepsilon_0\kappa_B T} \tag{4}$$

where ε_0 = permittivity of vacuum (8.854×10^{-12}), ε = permittivity of water (78.5), ζ = zeta potential, κ = Debye–Huckel reciprocal length, e = electron charge, n_i = ionic strength, z_i = counterion valence, κ_B = Boltzmann constant, and T = absolute temperature.

The current study utilized the conventional DLVO theory to understand the surface interactions between Fe_3O_4 NPs and sand in the environment. These interactions dictate the mobility of NPs within the soil matrix. While strong ES repulsion is expected to promote the dispersion of NPs, VDW forces favor the aggregation and trapping of NPs in soil. Using Eqs. (1)–(4), the interparticle interaction potentials between two Fe_3O_4 NPs were computed, which provides information on the transport and behavior of NPs in each environmental condition.

Results and discussion

Characterization of Fe_3O_4

The physicochemical properties of Fe_3O_4 NPs were thoroughly analyzed. The XRD measurements of iron oxide magnetic nanoparticles correspond to the reference value for Fe_3O_4 (JCPDS file number 65–3107). Fe_3O_4 exhibits well-defined Bragg reflection properties according to XRD examination of the particles (Fig. S1 A). The data displays diffraction angles of NPs at 2q = 30.103°, 35.451°, 43.088°, 53.516°, and 62.657°, indicating a characteristic crystal lattice structure and the presence of well-defined atomic planes within the NPs, emphasizing their composition and arrangement.

Fig. S1B indicates that the peak at 546 cm^{-1} is due to Fe–O stretching vibration on Fe_3O_4 NPs. The O causes the elevation at 3364 cm^{-1}–H stretching mode vibrations induced by hydroxyl groups on NPs in water. The band at 2967 cm^{-1} corresponds to asymmetric CH_2 stretching, indicating the presence of aliphatic chains on the surface, possibly from a surfactant used during the synthesis or stabilization process; 2320 cm^{-1} corresponding to C–O bending suggests the presence of metal–oxygen bonds, which can be attributed to the oxide layer on the surface of the particles; 1625 cm^{-1} corresponding to N–H stretching and bending suggests the presence of amino groups, which could be a result of functionalization with amino silane or other amine-containing molecules; and 1065 cm^{-1} corresponding to C–H stretching vibrations indicates the presence of hydrocarbon groups, which could come from the surfactant or organic residues left over from the synthesis process. These peak values are almost identical to the asserted values of Nurbas et al. (2017).

The Fe_3O_4 NPs were concatenated into irregular forms with no discernible structure, as revealed by SEM images

(Fig. S1C). The aggregates formed by these NPs have a porous, sponge-like morphology. As previously noted, the magnetic behavior of NPs tends to stick together during sample preparation for SEM analysis (Babu and Prabu 2011). Therefore, the exact size of the Fe_3O_4 NPs was challenging to obtain. The EDAX spectrum (Fig. S1D) confirms the presence of Fe and O in the sample. It is worth mentioning here that in the current study, the tests were conducted with various sizes of aggregates of the Fe_3O_4 NPs. The properties of these aggregates may differ from truly nano-sized particles (1–100 nm).

The UV–VIS spectra of Fe_3O_4 NP dispersion were measured with the absorbance maxima (λ_{max}) recorded at 370 nm. This technique assessed the concentration of Fe_3O_4 NP in each experimental condition, providing valuable insights into the size and stability of NPs in the solution. It is worth noting that a previous investigation also reported similar observations regarding the NP concentration (Chaki et al. 2015).

The pH_{PZC} of Fe_3O_4 in Milli-Q water was confirmed to be 7.16, as shown in the graph (Fig. S3), which is very close to the value of 7.27 as determined by previous researchers (Pogorilyi et al. 2017).

Transport of Fe_3O_4 NPs in aqueous media

Effect of initial pH

The sedimentation pattern of Fe_3O_4 NPs as a function of the initial pH of the medium under static conditions is shown in Fig. 1. The particles gradually aggregated and settled at three pH values (5, 7, and 9). In particular, at pH 7, near the PZC of NPs ($pH_{PZC} = 7.16$), the sedimentation rate of NPs was maximum, where the electrostatic repulsion between the NPs was significantly diminished (Khan et al. 2022; Thio et al. 2011). The relative sedimentation regimes at this particular pH are in concordance with the formation of large aggregates (> 1000 nm) as compared with other pH values (5 and 9), which resulted in smaller aggregates (< 600 nm) (Table S2). These measurements demonstrate the polydispersity in aggregate sizes under different pH conditions, highlighting the variation in aggregate behavior. At this pH, the Fe_3O_4 NPs had merely a low surface charge (− 7.73 mV), fostering their aggregation due to limited repulsive forces according to DLVO theory (Fig. 9A), which is in agreement with the previous experimental results (Baalousha 2009). The surface interactive forces between two Fe_3O_4 NPs were the greatest at pH 9 due to the deprotonation of surface functional groups; however, at pH 5, the surface charge of the NPs is less negative, which leads to weaker repulsive forces and a greater propensity for aggregation. It should be noted that the stability of the NP increased at pH 9 (− 26.82 mV) (Table S2). The considerable aggregation at pH 7 can be attributed to the enhanced interaction between the aggregates driven by differential sedimentation patterns over time (Illés and Tombácz 2006). The aggregate sedimentation was observed by the NP size (Table S2). The considerable aggregation and dispersion at these pH values can affect the surface charge of the NPs through protonation and deprotonation of the surface functional groups. Accordingly, solution pH is crucial in defining the transport profile of Fe_3O_4 NPs in aqueous mediums.

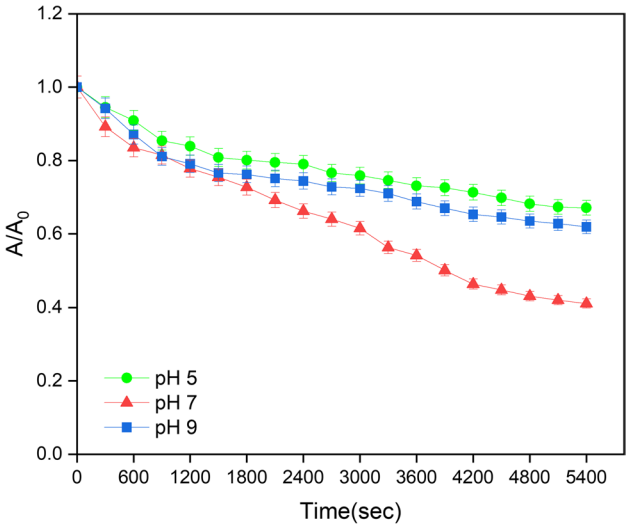

Fig. 1 Sedimentation profiles of Fe_3O_4 NPs in aqueous media with different pH (5, 7, and 9) conditions without IS and HA concentrations. The concentration of Fe_3O_4 NPs was 50 mg L^{-1}. Error bars indicate the standard deviation of triplicates

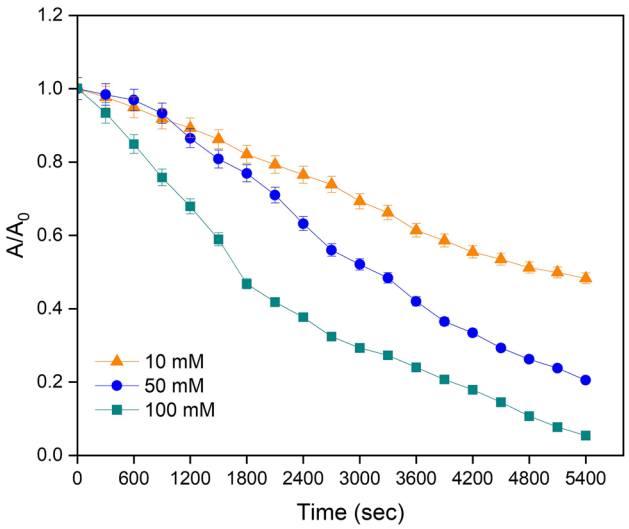

Fig. 2 Sedimentation profiles of Fe_3O_4 NPs in aqueous media with different IS (10, 50, 100 mM) conditions at pH 7 and absence of HA. The concentration of Fe_3O_4 NPs was 50 mg L^{-1}. Error bars indicate the standard deviation of triplicates

Effect of ionic strength

Figure 2 represents the sedimentation regimes of Fe_3O_4 NPs with different (IS) concentrations at pH 7. The sedimentation of NPs increased significantly as the solution IS increased from 10 to 100 mM. The enhanced aggregation due to the higher ionic strength led to increased sedimentation since there was less repulsive force between the NPs. The value of A/A_0 abruptly decreased as the IS of the background solution progressed from 10 to 100 mM. This was supported by the concurrent increase in the aggregate size (Table S2), indicating the destabilized Fe_3O_4 NPs in the suspension (Sodnikar et al. 2021). It must be noted that at a low IS (10 mM), the effective diameter of the aggregates was 1123 nm (under static conditions), which then increased to 1957 at high IS (100 nm) conditions. As the concentration of ions in the solution is raised, the EDL compression and the electrostatic repulsion among the NPs diminish, resulting in lower colloidal particle stability during transport (Ben-Moshe et al. 2010; Wang et al. 2008). Another plausible explanation is that the Na^+ ions at lower IS penetrated the static electric double layer and resulted in a higher screening of surface charge, and the charge neutralization promoted aggregation of Fe_3O_4 NPs. This is evident from the surface charge potential of Fe_3O_4 NPs, which is − 12.16 mV (Table S3). Therefore, the transport behavior of Fe_3O_4 NPs gets hindered as IS increases.

Effect of humic acid

The effects of HA on the transport behavior of Fe_3O_4 NPs were investigated at constant pH 7 (Fig. 3). HA induced steric stabilization due to the adsorption of negatively charged carboxylic and phenolic functional groups on the NP surface. As a result, the aquatic transport was enhanced, as marked by a higher A/A_0 ratio (Yang et al. 2009). The FT-IR spectrum analysis (Fig. S4) of the humic acid interacted Fe_3O_4 shows peaks at 1580 cm^{-1} and 1730 cm^{-1}, which corresponds to the C = O bond stretching and the presence of the COOH group, respectively (Fatema et al. 2015). All these functional groups confirm the adsorption of HA on the surface of Fe_3O_4. Different environmentally relevant concentrations of HA (0.1, 1.0, 10.0 mg L^{-1}) were employed in this study, and a steady A/A_0 ratio was acquired as the concentration of HA increased from 0.1 mg L^{-1} to 10 mg L^{-1}, indicating stable Fe_3O_4 suspension (Fig. 3). Under these circumstances, Fe_3O_4 NPs diffused in the background solution, and the aggregation was limited. The impact of transport enhancement of the Fe_3O_4 NPs was more prominent at the maximum HA concentration (10 mg L^{-1}). The influence of adsorption of relatively more HA onto the surface of Fe_3O_4 increased the negative charge on the NPs, which enhanced the A/A_0 ratio. The improved zeta potential value (− 33.25) (Table S2) indicates the presence of steric repulsion due to the adsorbed HA and the formation of a macromolecular layer around the Fe_3O_4 NPs (Tombácz et al. 2004). Similar impacts of HA on the sedimentation behavior of Fe_3O_4 NPs were observed in other studies (Amal et al. 1992; Baalousha 2009; Verrall et al. 1999). Thus, the adsorption of HA onto Fe_3O_4 NPs can enhance their stability and promote their transport in aqueous environments through surface coating, density, or charge neutralization (Hou et al. 2017; Zhang et al. 2015).

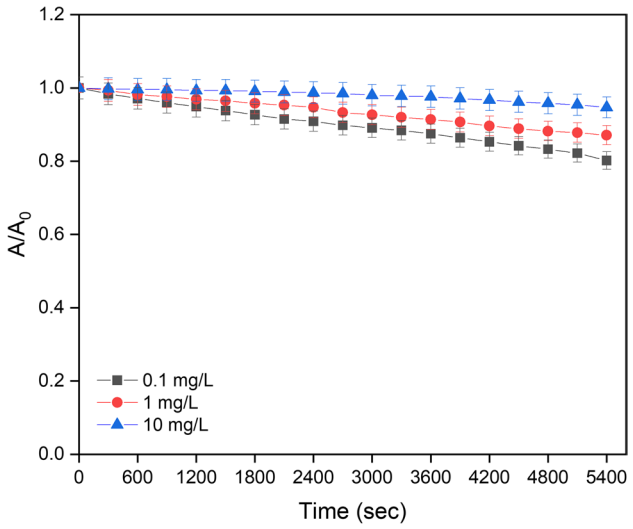

Fig. 3 Sedimentation profiles of Fe_3O_4 NPs in aqueous media with different HA concentrations (0.1, 1, 10 mg L^{-1}) at pH 7 and absence of IS. The concentration of Fe_3O_4 NPs was 50 mg L^{-1}. Error bars indicate the standard deviation of triplicates

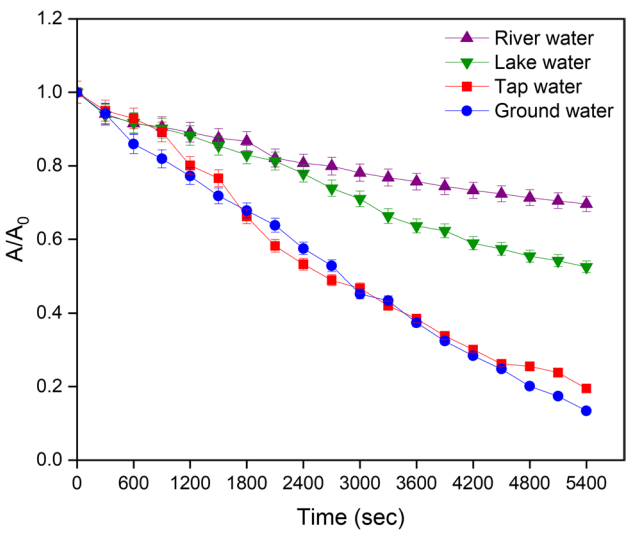

Fig. 4 Sedimentation profiles of Fe_3O_4 NPs in different natural waters (river, lake, tap, groundwater). The concentration of Fe_3O_4 NPs was 50 mg L^{-1}. Error bars indicate the standard deviation of triplicates

Transport behavior of Fe_3O_4 in various environmental water systems

The impact of different natural water solution chemistry was explored to gain a practical understanding of the transport behavior of Fe_3O_4 NPs in the aqueous system. Under all tested conditions, the A/A_0 ratio of Fe_3O_4 NPs slightly declined in the river and lake water. In contrast, a significant drop in the A/A_0 ratio was observed in both tap and groundwater (Fig. 4). The reasonably high stability of Fe_3O_4 NP suspension in river water and lake water was exhibited by the apparent zeta potential values of − 23.45 and − 17.87, respectively. The transport of NPs in river and lake water is quite complex because of the interplay between surface coating characteristics, presence and absence of NOM, and turbulent forces. Owing to the enhanced adsorption of various dissolved organic matter (DOM) from these natural waters onto the surface of Fe_3O_4 NPs, the thickness of the interfacial layer surrounding the NPs was greater than the Debye length, resulting in the van der Waals force of attraction being less prevalent than electrostatic repulsion among NPs. As a result, the stability of Fe_3O_4 NPs when suspended in these natural waters was confirmed, consistent with previous studies (Wang et al. 2008). The tap and ground water demonstrated exceptionally high sedimentation regimes, indicating low colloidal stability of the Fe_3O_4 dispersion. Tap water is characterized by a lower concentration of dissolved ions and organic carbon than other natural waters due to the typical ion composition in municipal water supplies, where the overall ion concentration is kept at lower levels. Fe_3O_4 NPs, in the presence of tap water, exhibited enhanced sedimentation due to the formation of large aggregates when the pH of the tap water was nearly close to its PZC (7.16). It implied that the absence of surface charge among Fe_3O_4 NPs enhanced the aggregate formation consequently, and lower A/A_0 ratios were observed. Groundwater, among all the studied natural waters, exhibited the greatest sedimentation over time with the formation of large aggregates of > 1900 nm. High concentrations of divalent ions (Mg^{2+} and Ca^{2+}) and lower concentrations of NOM in the groundwater enhanced the aggregation of Fe_3O_4 NPs (Conway et al. 2015; Lanphere et al. 2014).

Transport of Fe_3O_4 NPs in porous media

Effect of initial pH

The breakthrough curves of Fe_3O_4 NP suspension were shown in Fig. 5 at various initial pH levels (5, 7, and 9). The Fe_3O_4 NPs readily flow out of the column at pH values such as pH 5 and 9, where repulsive force arises due to the higher charge content between NPs and sand. The BTC of Fe_3O_4 suspension exhibited a rapid increase between pH 5 and 9 before plateauing; particularly, at pH 9, the proportional concentration in the column effluent almost reaches unity. This was due to the colloid deposition force inhibited by electrostatic repulsion on the sand surface. Conversely, lower repulsive forces at pH 7 (=PZC), where sand particles and colloids were mildly charged, enable colloidal Fe_3O_4 to adhere to the surface of the sand. Due to this, the effluent concentration remained stable without any significant increase. In the BTCs for pH 5 and 9 suspensions, a slight rise was seen at PV 12 due to the leaching of Fe_3O_4 from the porous media (maximum for pH 9). This suggested that Fe_3O_4 NPs and sand could bind reversibly. The transport recovery rates of Fe_3O_4 NPs at pH 5 and 9 were 94%

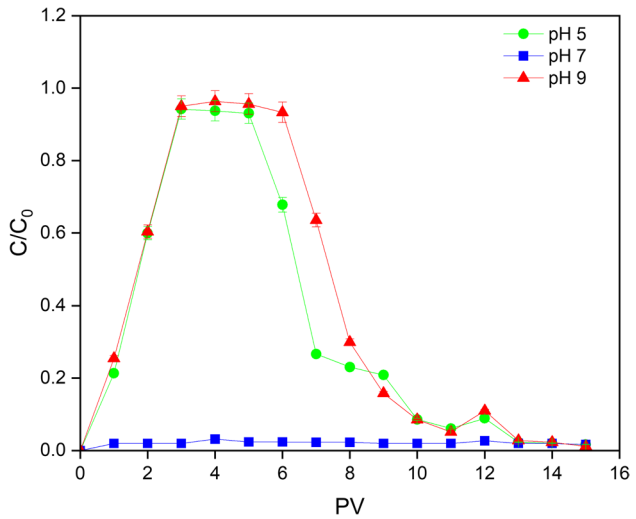

Fig. 5 The Breakthrough curve of Fe_3O_4 NPs in porous media with different pH (5, 7, and 9) conditions without IS and HA concentrations. The concentration of Fe_3O_4 NPs was 50 mg L^{-1}. Error bars indicate the standard deviation of triplicates

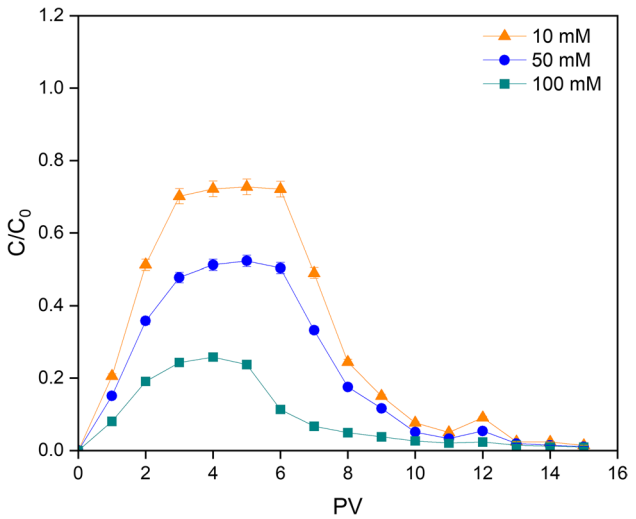

Fig. 6 The breakthrough curve of Fe_3O_4 NPs in porous media with different IS (10, 50, 100 mM) conditions at pH 7 and absence of HA. The concentration of Fe_3O_4 NPs was 50 mg L^{-1}. Error bars indicate the standard deviation of triplicates

and 96%, respectively, demonstrating a high transport rate and low deposition in sand. The MPs were forced apart because of the significant electrostatic double-layer (EDL) repulsion among the Fe_3O_4–sand particles and served as the crucial controlling factor. Due to these unfavorable circumstances, Fe_3O_4 NPs were restricted from attaching to the sand surface, resulting in improved mobility at pH 5 and 9. In contrast, the transport recovery rate was 3% for pH 7 suspension, suggesting high deposition of Fe_3O_4. Additionally, the C/C_0 value dropped to almost zero when the influent pH reached 7. This is due to the substantially larger Fe_3O_4 aggregate size (> 1000 nm), which led to severe straining and the blocking effect of the column near the inlet (Phenrat et al. 2009). The overall interaction energy across Fe_3O_4 and sand grains at pH 7 is attributed to the van der Waals attraction force according to the DLVO interaction profile depicted in Fig. 9. The deposited Fe_3O_4 NPs were most likely at the primary energy minima, indicating a significant interaction between the NPs and quartz sand. In addition, the restricted release of deposited Fe_3O_4 NPs exceeding 2 PVs supports the theory that the Fe_3O_4 NPs are accumulated at primary energy minima under favorable environmental pH, preventing the particles from releasing during subsequent DI water flushing. Overall, the repulsive charges on the NPs and sand surface were accountable for the increased mobility of Fe_3O_4 NPs at these pH levels.

Effect of ionic strength

The porous media transport profile of Fe_3O_4 NPs dispersed in solutions of varying concentrations of monovalent ions (Na^+) (10, 50, and 100 mM) at pH 7 is shown in Fig. 6. The C/C_0 ratio decreased as the ionic intensity of the influent increased. The maximum amount of Fe_3O_4 was eluted at IS of 10 mM, followed by 50 and 100 mM at PV 5 with transport recoveries of 72%, 52%, and 25%, respectively, demonstrating high retent, ion, and low propensity of Fe_3O_4 NPs. When the IS rises, the electrostatic double layers around the sand and Fe_3O_4 NPs become more compressed, reducing the repulsive forces between them (Franchi 2000, Nowack and Stone 1999). The apparent zeta potential results corroborate with these evaluations as it decreases from − 12.16 to − 4.26 mV. However, the effluent profiles in Fig. 6 show that increasing IS decreased the mobility and increased retention of Fe_3O_4 NPs, as in the column effluent. For all tests, the BTCs at PV 12 slightly increased due to the remobilization of Fe_3O_4 NPs in the quartz sand under these experimental conditions. The DLVO hypothesis makes idealized assertions and ignores the complexity of the Fe_3O_4 NP-sand system. The surface charge and other properties of NPs could change due to increased IS and altering their interaction with the soil matrix. In addition, other factors could interact with the effect of IS, further confounding the transport dynamics of Fe_3O_4 NPs, such as unique surface chemistry, surface roughness, and other forces like capillary and hydrodynamic interactions (Phenrat et al. 2010; Xu et al. 2020). The DLVO theory might not adequately account for these changes, which would cause a discrepancy between the expected interaction profile and the actual transport behavior.

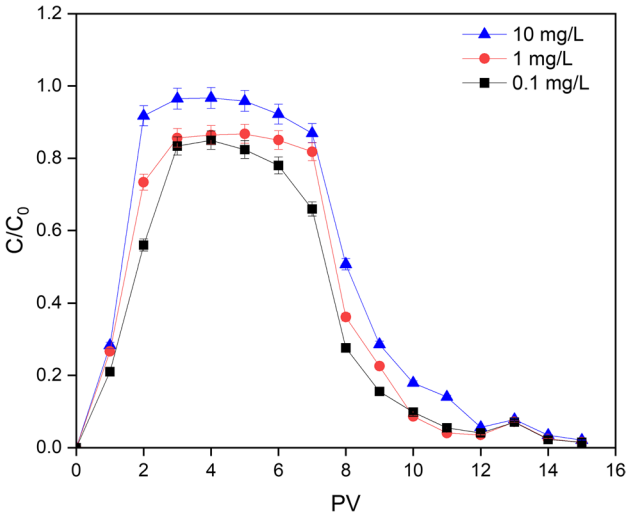

Fig. 7 The breakthrough curve of Fe_3O_4 NPs in porous media with different HA concentrations (0.1, 1, 10 mg L^{-1}) at pH 7 and absence of IS. The concentration of Fe_3O_4 NPs was 50 mg L^{-1}. Error bars indicate the standard deviation of triplicates

Effect of humic acid concentrations

The effect of natural organic matter on colloidal nanoparticles is a critical consideration in evaluating their fate and transport behavior (Hotze et al. 2010). Figure 7 shows the BTCs of Fe_3O_4 dispersed at pH 7 with various concentrations of HA (0.1, 1, and 10 mg L^{-1}). Under all test conditions, a high C/C_0 ratio (~ > 0.9) and comparatively high breakthrough time (up to 6 PVs) were observed for 10 mg L^{-1} HA concentration, demonstrating low retention and significant mobility of Fe_3O_4 in the column. A high rate of elution of Fe_3O_4 NPs was observed in 10 mg L^{-1}, proceeded by 1 and 0.1 mg L^{-1} at PV1, and the respective transport recovery rates from the column effluent were 96%, 86%, and 84%. The ions of Fe_3O_4 from porous media may have caused a slight peak at PV 12 for all HA concentrations. A comparative reduction in the hydrodynamic size of Fe_3O_4 was noted as the HA concentration increased (Table S2). This agrees with the previous results (Wang et al. 2020). In addition to preventing aggregation, HA adsorption onto the surface of Fe_3O_4 NPs aids in the dispersion of the colloidal particles in the solution. However, HA had a negligible effect on the zeta potential (Table S2) and DLVO energy profiles

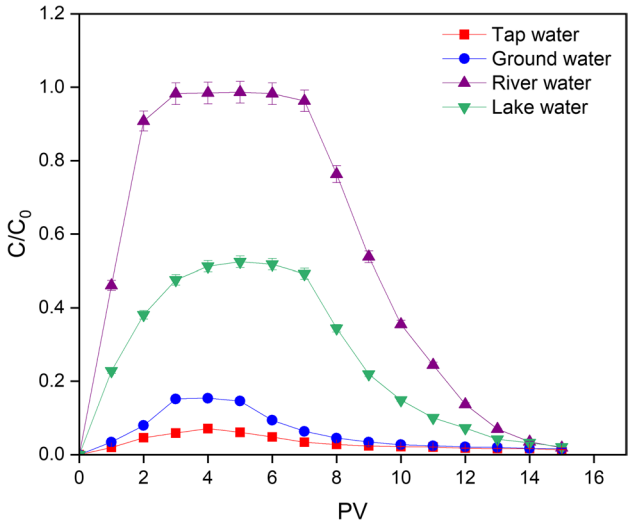

Fig. 8 The breakthrough curve of Fe_3O_4 NPs in different natural waters (river, lake, tap, groundwater) through porous media. The concentration of Fe_3O_4 NPs was 50 mg L^{-1}. Error bars indicate the standard deviation of triplicates

(Fig. 9C), indicating the influence of other dominating colloidal interactions. The likely mechanism is that the thermodynamic interaction between sand particles and organic matter–Fe_3O_4 NP complexation could overcome the interaction energy barrier and inhibit their retention in the porous media, thus inducing electrostatic stability in the dispersion. Gu et al. proposed that the prominent interplay between iron oxide and NOM is the ligand exchange and electrostatic interactions among the surface hydroxyl groups of Fe_3O_4 and the carboxyl or hydroxyl groups in natural organic matter of most systems (Gu et al. 1994). The interaction between Fe_3O_4 NPs and NOM in the porous media could potentially affect the colloidal transport of Fe_3O_4 NPs.

Transport behavior of Fe_3O_4 NPs in various natural water systems

Figure 8 indicates the porous media transport of Fe_3O_4 NPs in different environmental water systems. For various environmental water samples, the breakthrough was achieved at PV 1 for river and lake waters and PV 2 for groundwater. No breakthrough point was defined in tap water, indicating high retention. A strong C/C_0 ratio of 0.97 was observed in river water, indicating an increased mobility of NPs. This suggests that the high concentration of dissolved ions in river water reduces NP retention. Conversely, a lower C/C_0 ratio of 0.48 was observed in the presence of lake water, indicating reduced mobility of NPs. This can be attributed to the lower concentration of dissolved ions in lake water, which promotes NP retention. Fe_3O_4 in the presence of ground and tap water exhibited a C/C_0 ratio of 0.12 and 0.08, respectively, which signifies a very high deposition of nanoparticles in the column. The transport recovery rate of Fe_3O_4 NPs from the column outlet was 98%, 52%, 15%, and 7% for river, lake, ground, and tap water, respectively. River water has the highest mobility, followed by lake and groundwater. Tap water shows the least transport behavior in porous media with high retention in sand columns among the tested water samples, which follows the same trend as the transport in aqueous media.

The considerable abundance of organic matter in river and lake water was confirmed by total organic carbon measurements (Table S1) adsorbed to the surface of Fe_3O_4, which repels negatively charged sand particles and hinders particle retention (Phenrat et al. 2008). Thus, the presence of NOM augmented the transport and stability of Fe_3O_4 colloids through electrostatic and steric interactions. As per the literature studies, the quantity and dispersion of surface hydroxyl groups on iron oxide particle suspension make them sensitive to the adsorption of organic matter and ions (Gu et al.

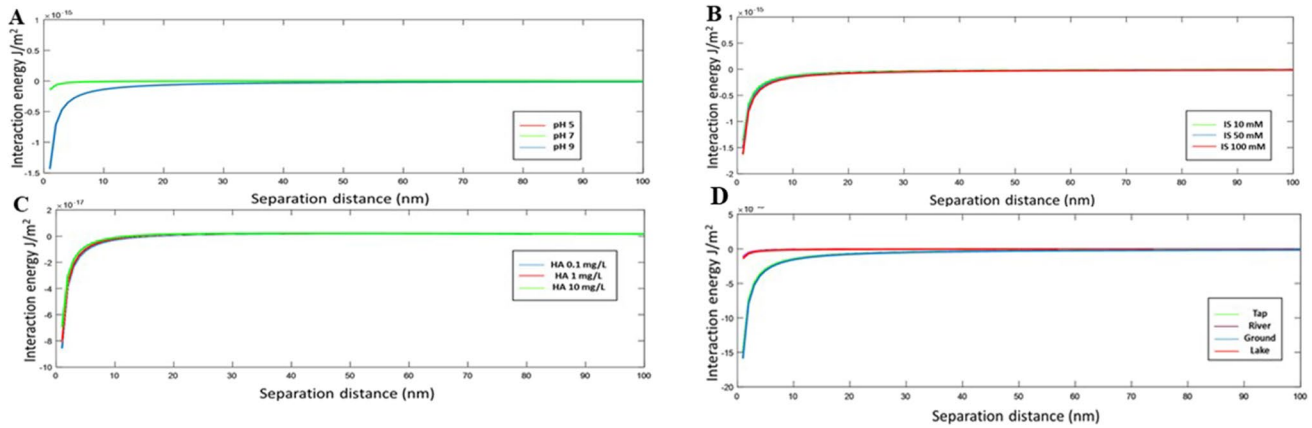

Fig. 9 The DLVO energy profiles of Fe_3O_4 NPs under various conditions A with different pH values (5, 7, and 9), B with different IS (10, 50, and 100 mM), C with different HA concentrations (0.1, 1, and 10 mg L^{-1}), and D in different environmental waters (river, lake, tap, and groundwater)

1994; Sun et al. 2023). Thus, dispersing the Fe_3O_4 in river and lake water plausibly exposed these surface hydroxyl groups to the humic acid, and monovalent ions in the water systems minimized the EDL compression and enhanced the electrostatic repulsion among Fe_3O_4 NPs according to the DLVO interactive energy profiles (Fig. 9D). The interactive force between the Fe_3O_4 NPs and NOM overcomes the energy barrier between the NP and sand, thus enhancing their transport. The high particle retention in tap water and groundwater is due to the potential aggregation and straining effects of Fe_3O_4. The pH of the tap water (7.7 ~ = PZC) can influence the changes in the electrostatic interactions, affecting the retention behavior of Fe_3O_4 NPs in porous media. Due to the high ionic strength of the groundwater (Table S1), they could be adsorbed onto porous media and inhibit the transportability of Fe_3O_4. Understanding the possible behavior and transport of Fe_3O_4 NPs in these natural environmental conditions aids in estimating the risk levels of exposure scenarios.

DLVO interaction energy interpretation

The DLVO interaction energies of Fe_3O_4 NPs were calculated to determine the mechanism underlying NP's subsequent sedimentation and deposition in the porous media. Figure 9A shows the effect of different pHs on the total interaction energy of Fe_3O_4 NPs. According to the DLVO theory, Fe_3O_4 NPs have a negative interaction energy pattern at pH 7, and as the separation gap between the two Fe_3O_4 NPs increased, it approached zero. The existence of significant van der Waals force among Fe_3O_4 NPs, as suggested by the absence of an energy barrier (Φmax) and larger primary minimum value (Φ_{min}) (−1.437E-15), led to the considerable sedimentation and deposition in the aqueous matrix. A positive interaction energy profile was found at pH 5 and 9, and the Φ_{min} decreased dramatically, suggesting that van der Waals's attractive force was diminishing. As the overall NP interaction energy was repulsive, the Fe_3O_4 NPs exhibited enhanced stability at pH 5 and 9. As a result, Fe_3O_4 NPs disseminated in suspensions of pH 5 and 9 had greater sedimentation and deposition ratios as compared to those dispersed in solutions of pH 7.

Fe_3O_4 NPs dispersed in the aqueous matrix at 10, 50, and 100 mM ionic concentrations exhibited a negative interaction energy profile. Figure 9B shows the impact of various IS on the total interaction energy of Fe_3O_4 NPs. The Φ_{min} increased gradually with the rise in the ion concentration in solution from 10 to 100 mM. The higher Φ_{min} values support the observed colloidal instability under all test conditions. According to the findings, adding higher salt concentration enhanced the van der Waals forces among Fe_3O_4 NPs owing to EDL compression. Consequently, an increased aggregation, sedimentation, and deposition rate was observed in the aqueous matrix. Therefore, the A/A_0 ratios increased remarkably with a rise in the IS from 10 to 100 mM.

Figure 9C depicted a positive interaction energy pattern when Fe_3O_4 NPs dispersed in a background solution containing humic acid at varying concentrations (0.1, 1, and 10 mg L^{-1}). The Φ_{min} tended to decrease, and an increment in maximum energy barriers (Φ_{max}) was observed with rising concentrations of HA. According to the DLVO interaction energy profile, the presence of HA at various concentrations augmented the electrostatic and steric repulsion among NPs due to its surface adsorption. As a result, a higher energy barrier prevented Fe_3O_4 aggregation and retention in the aqueous environment, thereby increasing the stability and transportability of Fe_3O_4 NPs, which correlates to the high absorbance values.

Fe_3O_4 NPs were suspended in various natural waters (river, lake, tap, and groundwater) (Fig. 9D). A positive interaction energy profile was obtained between the NPs when suspended in the river and lake water systems. In contrast, the overall interaction energy of Fe_3O_4 NPs suspended in ground and tap water was negative. When suspended in lake and river water, the decreased Φ_{min} of Fe_3O_4 NPs indicated the presence of strong stearic repulsion among NPs due to the adsorption of NOM on the nanoparticle surface. The increased steric repulsion due to increased Φ_{max} between NPs contributed to its stability in the presence of lake and river water. In tap and groundwater, the increased Φ_{min} of Fe_3O_4 NPs suggested that the van der Waals attraction force was dominant among NPs due to EDL compression. As a result, aggregation, sedimentation, and deposition of Fe_3O_4 NPs were observed in lake and river water under a porous matrix, which corresponded to lower absorbance ratios.

Conclusion

The findings of this study demonstrated that the transport profiles of Fe_3O_4 NPs in aquatic and porous media are controlled by various solution chemistry factors. The results showed that Fe_3O_4 NPs behave distinctly under different pH, IS, and HA conditions. The interactive forces on the surface of Fe_3O_4 NPs, electron double-layer repulsion, and electrostatic and steric interactions were the major phenomena responsible for the transport of Fe_3O_4 NPs. An abrupt change in the surface chemistry may cause aggregation or trigger the release of previously adsorbed NPs into the water. Aggregation and sedimentation can cause the NPs to settle in the bottom sediments, reducing their mobility and potential exposure to biota. Furthermore, if Fe_3O_4 NPs dissolve, Fe ions can be released, sometimes leading to potential ecological risks. It is important to note that the surface modification of NPs can significantly alter their interactions with the environment and biota, which can further impact their toxicity and uptake. Analyzing the complete transport phenomena of Fe_3O_4 NPs is essential to

predict their environmental risks. These trends, however, may be disguised by the existence of several other physicochemical processes occurring in the environment. Thus, additional research is necessary to delineate conceptual models and to systematically evaluate all potential interaction concepts for predicting the fate and transport of NPs.

Supplementary Information The online version contains supplementary material available at https://doi.org/10.1007/s11356-023-30628-z.

Acknowledgements The authors thank the Centre for Fire, Explosives, and Environment Safety, Timarpur, Delhi 110054, India, and the Vellore Institute of Technology (VIT) for providing the nanomaterials and SEM facilities used in this study. The authors would also like to thank Sh. Rajiv Narang (Outstanding Scientist and Director), Centre for Fire, Explosives, and Environment Safety-Defence Research and Development Organisation (CFEES-DRDO) for funding this research (Sanction No. CFEES/TCP/EnSG/CARS(P)/DG(SAM)/FTS-ERAF/VIT-VELLORE).

Author contribution Reetha Thomas: methodology and writing—review and editing

Debayan Ghosh: investigation, methodology, visualization, formal analysis, and writing—original draft

Mrudula Pulimi: conceptualization, methodology, supervision, and writing—review and editing

M. Joyce Nirmala: writing—review and editing

Shalini Anand: conceptualization, methodology, and writing—review and editing

Pramod Kumar Rai: conceptualization and writing—review and editing

Amitava Mukherjee: conceptualization, methodology, supervision, project administration, and writing—review and editing

Funding The study was carried out using the funds provided by CFEES-DRDO (Sanction No. CFEES/TCP/EnSG/CARS(P)/DG(SAM)/FTS-ERAF/VIT-VELLORE).

Data availability All data employed in support of the study's outcomes are included in the article.

Declarations

Ethical approval Not applicable.

Informed consent It is declared that the study involved no human participants.

Consent to participate Not applicable.

Consent for publication All authors have given consent to the publication of the manuscript.

Competing interests The authors declare no competing interests.

References

Ali A, Zafar H, Zia M, ul Haq I, Phull AR, Ali JS, Hussain A, (2016) Synthesis, characterization, applications, and challenges of iron oxide nanoparticles. Nanotechnol Sci Appl 49–67. https://doi.org/10.2147/NSA.S99986

Amal R, Raper JA, Waite T (1992) Effect of fulvic acid adsorption on the aggregation kinetics and structure of hematite particles. J Colloid Interface Sci 151:244–257

Baalousha M (2009) Aggregation and disaggregation of iron oxide nanoparticles: influence of particle concentration, pH and natural organic matter. Sci Total Environ 407:2093–2101

Babu SA, Prabu HG (2011) Synthesis of AgNPs using the extract of Calotropis procera flower at room temperature. Mater Lett 65:1675–1677

Ben-Moshe T, Dror I, Berkowitz B (2010) Transport of metal oxide nanoparticles in saturated porous media. Chemosphere 81:387–393

Carstens JF, Bachmann J, Neuweiler I (2017) Effects of flow interruption on transport and retention of iron oxide colloids in quartz sand. Colloids Surf, A 520:532–543

Chaki S, Malek TJ, Chaudhary M, Tailor J, Deshpande M (2015) Magnetite Fe3O4 nanoparticles synthesis by wet chemical reduction and their characterization. Adv Nat Sci: Nanosci Nanotechnol 6:035009

Chekli L, Phuntsho S, Roy M, Lombi E, Donner E, Shon HK (2013) Assessing the aggregation behaviour of iron oxide nanoparticles under relevant environmental conditions using a multi-method approach. Water Res 47:4585–4599

Chen M, Tao X, Wang D, Xu Z, Xu X, Hu X, Xu N, Cao X (2019) Facilitated transport of cadmium by biochar-Fe3O4 nanocomposites in water-saturated natural soils. Sci Total Environ 684:265–275

Conway JR, Adeleye AS, Gardea-Torresdey J, Keller AA (2015) Aggregation, dissolution, and transformation of copper nanoparticles in natural waters. Environ Sci Technol 49:2749–2756

Daoush WM (2017) Co-precipitation and magnetic properties of magnetite nanoparticles for potential biomedical applications. J Nanomed Res 5:00118

Dibyanshu K, Chhaya T, Raychoudhury T (2022) A review on the fate and transport behavior of engineered nanoparticles: possibility of becoming an emerging contaminant in the groundwater. Int J Environ Sci Technol 20:4649–4672. https://doi.org/10.1007/s13762-021-03835-9

Ding Y, Bai X, Ye Z, Ma L, Liang L (2019) Toxicological responses of Fe3O4 nanoparticles on Eichhornia crassipes and associated plant transportation. Sci Total Environ 671:558–567

Elias S, Alderton D (2020) Encyclopedia of geology. Academic Press, p 5622

Fatema J, Bhattacharjee S, Pernitsky D, Maiti A (2015) Study of the aggregation behavior of silica and dissolved organic matter in oil sands produced water using Taguchi experimental design. Energy Fuels 29:7465–7473

FazeliSangani M, Owens G, Fotovat A (2019) Transport of engineered nanoparticles in soils and aquifers. Environ Rev 27:43–70

Franchi A (2000) Deposition and reentrainment of colloids in porous media: effects of natural organic matter and solution chemistry. The Johns Hopkins University, 9964098

Galloway TS, Cole M, Lewis C (2017) Interactions of microplastic debris throughout the marine ecosystem. Nat Ecol Evol 1:0116

Ghosh D, Das S, Gahlot VK, Pulimi M, Anand S, Chandrasekaran N, Rai PK, Mukherjee A (2022) A comprehensive estimate of the aggregation and transport of nSiO 2 in static and dynamic aqueous systems. Environ Sci Process Impacts 24:675–688

Goswami L, Kim K-H, Deep A, Das P, Bhattacharya SS, Kumar S, Adelodun AA (2017) Engineered nano particles: nature, behavior, and effect on the environment. J Environ Manag 196:297–315

Gu B, Schmitt J, Chen Z, Liang L, McCarthy JF (1994) Adsorption and desorption of natural organic matter on iron oxide: mechanisms and models. Environ Sci Technol 28:38–46

Herrera-Barros A, Bitar-Castro N, Villabona-Ortíz Á, Tejada-Tovar C, González-Delgado ÁD (2020) Nickel adsorption from aqueous

solution using lemon peel biomass chemically modified with TiO2 nanoparticles. Sustain Chem Pharm 17:100299
Hotze EM, Phenrat T, Lowry GV (2010) Nanoparticle aggregation: challenges to understanding transport and reactivity in the environment. J Environ Qual 39:1909–1924
Hou J, Zhang M, Wang P, Wang C, Miao L, Xu Y, You G, Lv B, Yang Y, Liu Z (2017) Transport, retention, and long-term release behavior of polymer-coated silver nanoparticles in saturated quartz sand: the impact of natural organic matters and electrolyte. Environ Pollut 229:49–59
Illés E, Tombácz E (2006) The effect of humic acid adsorption on pH-dependent surface charging and aggregation of magnetite nanoparticles. J Colloid Interface Sci 295:115–123
Imran M, Affandi AM, Alam MM, Khan A, Khan AI (2021) Advanced biomedical applications of iron oxide nanostructures based ferrofluids. Nanotechnology 32:422001
Kahlon SK, Sharma G, Julka J, Kumar A, Sharma S, Stadler FJ (2018) Impact of heavy metals and nanoparticles on aquatic biota. Environ Chem Lett 16:919–946
Khan B, Nawaz M, Price GJ, Hussain R, Waseem M, Haq S, Rehman W (2022) Effect of pH on the morphology of magnetite nanoparticles for adsorption of Cr (VI) ions from aqueous medium. J Dispers Sci Technol 44(9):1770–1777. https://doi.org/10.1080/01932691.2022.2053705
Kumar S, Kumar M, Singh A (2021) Synthesis and characterization of iron oxide nanoparticles (Fe2O3, Fe3O4): a brief review. Contemp Phys 62:144–164
Lanphere JD, Rogers B, Luth C, Bolster CH, Walker SL (2014) Stability and transport of graphene oxide nanoparticles in groundwater and surface water. Environ Eng Sci 31:350–359
Lei C, Sun Y, Tsang DC, Lin D (2018) Environmental transformations and ecological effects of iron-based nanoparticles. Environ Pollut 232:10–30
Li M, He L, Zhang M, Liu X, Tong M, Kim H (2019) Cotransport and deposition of iron oxides with different-sized plastic particles in saturated quartz sand. Environ Sci Technol 53:3547–3557
Ling X, Yan Z, Liu Y, Lu G (2021) Transport of nanoparticles in porous media and its effects on the co-existing pollutants. Environ Pollut 283:117098
Lu J, Liu D, Yang X, Liu H, Liu S, Tang H, Zhao Y, Cui F (2016) Sedimentation of TiO2 nanoparticles in aqueous solutions: influence of pH, ionic strength, and adsorption of humic acid. Desalin Water Treat 57:18817–18824
Lv B, Wang C, Hou J, Wang P, Miao L, Li Y, Ao Y, Yang Y, You G, Xu Y (2016) Influence of shear forces on the aggregation and sedimentation behavior of cerium dioxide (CeO 2) nanoparticles under different hydrochemical conditions. J Nanopart Res 18:1–12
Ma C, Huangfu X, He Q, Ma J, Huang R (2018) Deposition of engineered nanoparticles (ENPs) on surfaces in aquatic systems: a review of interaction forces, experimental approaches, and influencing factors. Environ Sci Pollut Res 25:33056–33081
Meng X, Yang D (2019) Critical review of stabilized nanoparticle transport in porous media. J Energy Resour Technol 141(7):070801
Mondal A, Dubey BK, Arora M, Mumford K (2021) Porous media transport of iron nanoparticles for site remediation application: a review of lab scale column study, transport modelling and field-scale application. J Hazard Mater 403:123443
Naz M, Bouzroud S, Raza MA, Tariq M, Fan X (2022) Metal oxide nanoparticles toxicity testing on terrestrial plants, Toxicity of Nanoparticles in Plants. Elsevier, pp 317–331. https://doi.org/10.1016/B978-0-323-90774-3.00013-1
Nowack B, Stone AT (1999) Adsorption of phosphonates onto the goethite–water interface. J Colloid Interface Sci 214:20–30
Nurbas M, Ghorbanpoor H, Avci H (2017) An eco-friendly approach to synthesis and characterization of magnetite (Fe3O4) nanoparticles using Platanus orientalis L. leaf extract. Dig J Nanomater Biostructures (DJNB) 12:993–1000
Ouyang S, Li Y, Zheng T, Wu K, Wang X, Zhou Q (2022) Ecotoxicity of natural nanocolloids in aquatic environment. Water 14:2971
Phenrat T, Saleh N, Sirk K, Kim H-J, Tilton RD, Lowry GV (2008) Stabilization of aqueous nanoscale zerovalent iron dispersions by anionic polyelectrolytes: adsorbed anionic polyelectrolyte layer properties and their effect on aggregation and sedimentation. J Nanopart Res 10:795–814
Phenrat T, Kim H-J, Fagerlund F, Illangasekare T, Tilton RD, Lowry GV (2009) Particle size distribution, concentration, and magnetic attraction affect transport of polymer-modified Fe0 nanoparticles in sand columns. Environ Sci Technol 43:5079–5085
Phenrat T, Cihan A, Kim H-J, Mital M, Illangasekare T, Lowry GV (2010) Transport and deposition of polymer-modified Fe0 nanoparticles in 2-D heterogeneous porous media: effects of particle concentration, Fe0 content, and coatings. Environ Sci Technol 44:9086–9093
Pogorilyi RP, Pylypchuk I, Melnyk IV, Zub YL, Seisenbaeva GA, Kessler VG (2017) Sol-gel derived adsorbents with enzymatic and complexonate functions for complex water remediation. Nanomaterials 7:298
Popescu RC, Andronescu E, Vasile BS (2019) Recent advances in magnetite nanoparticle functionalization for nanomedicine. Nanomaterials 9:1791
Shukla A, Patra MK, Mathew M, Songara S, Singh VK, Gowd GS, Vadera SR, Kumar N (2010) Preparation and characterization of biocompatible and water-dispersible superparamagnetic iron oxide nanoparticles (SPIONs). Adv Sci Lett 3:161–167
Sodnikar K, Parker KM, Stump SR, ThomasArrigo LK, Sander M (2021) Adsorption of double-stranded ribonucleic acids (dsRNA) to iron (oxyhydr-) oxide surfaces: comparative analysis of model dsRNA molecules and deoxyribonucleic acids (DNA). Environ Sci Process Impacts 23:605–620
Sun X-L, Wang Y, Xiong H-Q, Wu F, Lv T-X, Fang Y-C, Xiang H (2023) The role of surface functional groups of iron oxide, organic matter, and clay mineral complexes in sediments on the adsorption of copper ions. Sustainability 15:6711
Thio BJR, Zhou D, Keller AA (2011) Influence of natural organic matter on the aggregation and deposition of titanium dioxide nanoparticles. J Hazard Mater 189:556–563
Tombácz E, Libor Z, Illés E, Majzik A, Klumpp E (2004) The role of reactive surface sites and complexation by humic acids in the interaction of clay mineral and iron oxide particles. Org Geochem 35:257–267
Tong M, He L, Rong H, Li M, Kim H (2020) Transport behaviors of plastic particles in saturated quartz sand without and with biochar/Fe3O4-biochar amendment. Water Res 169:115284
Verrall KE, Warwick P, Fairhurst AJ (1999) Application of the Schulze-Hardy rule to haematite and haematite/humate colloid stability. Colloids Surf, A 150:261–273
Vindedahl AM, Strehlau JH, Arnold WA, Penn RL (2016) Organic matter and iron oxide nanoparticles: aggregation, interactions, and reactivity. Environ Sci Nano 3:494–505
Wang M, Lu T, Chen W, Zhang H, Qi W, Song Y, Qi Z (2020) Enhanced role of humic acid on the transport of iron oxide colloids in saturated porous media under various solution chemistry conditions. Colloids Surf, A 607:125486
Wang X, Dan Y, Diao Y, Liu F, Wang H, Sang W, Zhang Y (2022) Transport characteristics of polystyrene microplastics in saturated porous media with biochar/Fe3O4-biochar under various chemical conditions. Sci Total Environ 847:157576
Wang Y, Li Y, Fortner JD, Hughes JB, Abriola LM, Pennell KD (2008) Transport and retention of nanoscale C60 aggregates in water-saturated porous media. Environ Sci Technol 42:3588–3594

Xu S, Shen C, Zhang X, Chen X, Radosevich M, Wang S, Zhuang J (2020) Mobility of cellulose nanocrystals in porous media: effects of ionic strength, iron oxides, and soil colloids. Nanomaterials 10:348

Yang K, Lin D, Xing B (2009) Interactions of humic acid with nanosized inorganic oxides. Langmuir 25:3571–3576

Yu S-j, Yin Y-g, Chao J-b, Shen M-h, Liu J-f (2014) Highly dynamic PVP-coated silver nanoparticles in aquatic environments: chemical and morphology change induced by oxidation of Ag0 and reduction of Ag+. Environ Sci Technol 48:403–411

Zhang R, Zhang H, Tu C, Hu X, Li L, Luo Y, Christie P (2015) Facilitated transport of titanium dioxide nanoparticles by humic substances in saturated porous media under acidic conditions. J Nanopart Res 17:1–11

Zheng X, Li Y, Chen D, Zheng A, Que Q (2019) Study on analysis and sedimentation of alumina nanoparticles. Int J Environ Res Public Health 16:510